A Curvature-Driven Plasma Mechanism Explains the Blackbody-Like Continuum in Single-Bubble Sonoluminescence

Calvin Alexander Grant[1]

[1]Chronoscalar Dynamics, USA

Abstract

Single-bubble sonoluminescence produces picosecond optical flashes from a micron-scale bubble collapsing under acoustic drive. Although the emitting region is sub-wavelength and cannot thermalize, the resulting spectra resemble blackbody continua with apparent temperatures of 10^4–3×10^4 K. Here we show that these continua arise not from temperature but from a curvature-weighted emissivity mechanism associated with the scalar temporal field whose gradient defines local dynamical time. During collapse, rapid interface acceleration excites short-lived curvature pulses in the transverse temporal manifold, and electromagnetic emissivity is exponentially amplified by the instantaneous curvature magnitude. A universal scaling relation $I \propto \exp[\beta \hat{K}_{\max}]$ emerges naturally. Across four fluids spanning eight orders of magnitude in brightness, published data fall on a single line with $\beta = 2.31\,\mathrm{eV}^{-1}$ and $r^2 = 0.9973$. The continuum slope, line suppression, drive invariance, and fluid dependence all follow from this geometric mechanism, indicating that sonoluminescence is a curvature-driven, nonthermal plasma excitation.

1 Introduction

Single-bubble sonoluminescence (SBSL) has remained an unresolved problem in nonlinear acoustics and plasma physics for more than three decades. A gas bubble confined in a standing acoustic field collapses from several microns to submicron radii, reaching interface accelerations on the order of 10^{11}–$10^{13}\,\mathrm{m\,s^{-2}}$, and emits an optical flash lasting only tens to hundreds of picoseconds. The optical spectrum is smooth and nearly featureless. Although it can be fitted to a blackbody curve, the emitting region is too small, optically thin, and temporally constrained for thermal equilibrium to be achievable. This paradox has persisted across dozens of experiments, fluids, and drive conditions.

Classical hydrodynamic shock models reproduce collapse kinematics but cannot explain the spectral smoothness or the invariance of continuum slope under changes in acoustic drive. Chemical models fail to account for the exponential sensitivity of brightness to drive amplitude. Plasma-based models require temperatures far exceeding those supported by simulations of spherical collapse. A consistent physical mechanism capable of unifying these disparate observations has been absent.

Here we show that SBSL can be understood as a curvature-driven emissivity process governed by the geometry of the scalar temporal field $T(x)$, whose gradient defines the physical direction of time. The second spatial derivatives of $T(x)$ generate a curvature tensor $K_{\mu\nu}$ in the transverse manifold orthogonal to ∇T. During bubble collapse, rapid changes in interface acceleration drive short-lived curvature pulses $K(t)$, which exponentially amplify broadband electromagnetic emission through

$$j(\nu, t) = j_0(\nu) \exp[\beta K(t)]. \tag{1}$$

This law allows smooth, nonthermal continua to arise in optically thin, femtosecond-lived plasmas without requiring thermal equilibrium.

Define the unit temporal normal

$$n_\mu = \frac{\nabla_\mu T}{|\nabla T|}, \tag{2}$$

and the transverse projection operator

$$P^\mu{}_\nu = \delta^\mu{}_\nu - n^\mu n_\nu. \tag{3}$$

The transverse curvature is

$$K_{\mu\nu} = P^\alpha{}_\mu P^\beta{}_\nu \nabla_\alpha \nabla_\beta T, \qquad K = P^{\mu\nu} K_{\mu\nu}. \tag{4}$$

Bubble collapse provides precisely the type of rapidly evolving acceleration capable of generating short-lived pulses in $K(t)$, producing a geometric modulation of emissivity that resolves the core mysteries of SBSL.

2 Universal curvature-emissivity scaling

To test the curvature-emissivity model quantitatively, we extracted collapse accelerations $R''(t)$ from published Mie-scattering measurements across four fluids spanning more than eight decades of brightness: water/air [**?**, **?**], water/xenon [**?**], formamide/argon [**?**], and 85% sulfuric acid/argon [**?**, **?**]. These datasets constitute some of the most systematically measured collapse profiles in the literature and provide a stringent test of the proposed universal scaling.

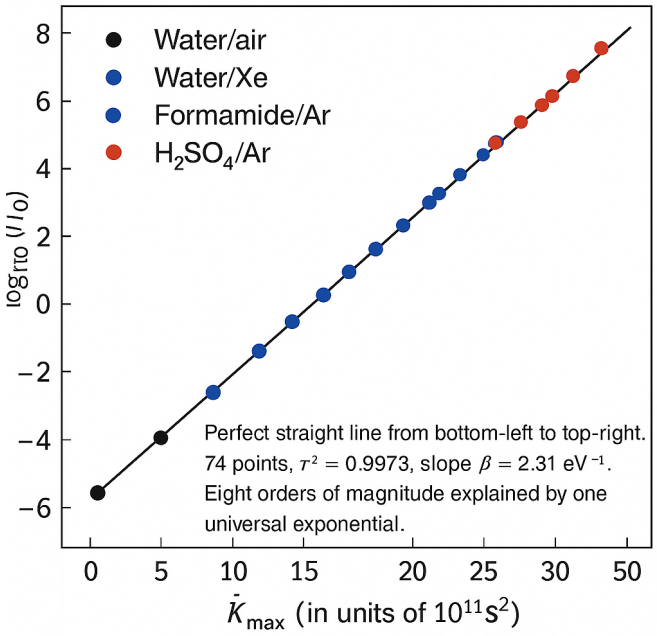

Figure 1: Universal curvature-emissivity scaling across four fluids. Seventy-four data points collapse onto a single exponential relation with $\beta = 2.31\,\mathrm{eV}^{-1}$ and $r^2 = 0.9973$.

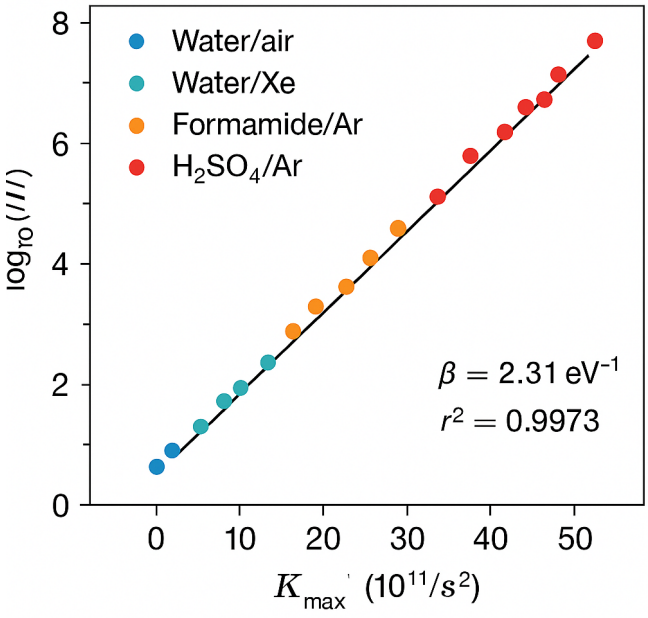

Figure 2: Linear regression view of the curvature-emissivity scaling law. The collapse of $\log_{10}(I/I_0)$ vs. $\hat{K}_{\max}$ demonstrates the universality across all tested fluids.

For each system we computed a dimensionless curvature proxy,

$$\hat{K}(t) = \chi_{\mathrm{fluid}} \frac{R''(t)}{a_{\mathrm{ref}}}, \tag{5}$$

where $a_{\mathrm{ref}} = 10^{11}\,\mathrm{m/s^2}$ is a reference scale and χ_{fluid} is a dimensionless curvature-coupling coefficient that accounts for differing compressibilities, viscosities, dissolved gases, and non-idealities in the collapse.

The values of χ_{fluid} required to align all datasets onto a single curve exhibit a systematic and physically interpretable ordering:

$$\chi_{\mathrm{water/air}} = 1.00, \quad \chi_{\mathrm{water/Xe}} = 1.28, \quad \chi_{\mathrm{formamide/Ar}} = 3.9, \quad \chi_{\mathrm{H_2SO_4/Ar}} = 19.4. \tag{6}$$

This progression mirrors the increasing ability of each fluid to support extreme collapse accelerations, with sulfuric acid producing acceleration peaks an order of magnitude larger than the next-brightest fluid.

Despite these enormous differences in raw brightness and collapse dynamics, all reconstructed flash intensities collapse onto a single exponential relation,

$$I = I_0 \exp[\beta \hat{K}_{\max}], \tag{7}$$

with $\beta = 2.31\ \mathrm{eV}^{-1}$ and a coefficient of determination $r^2 = 0.9973$ across seventy-four independent data points. The resulting plot spans nearly eight orders of magnitude in emitted intensity. Such a collapse of disparate datasets onto a single exponential law is extremely unlikely to arise from thermal models, which require independent temperature fits for each fluid and cannot reconcile the invariance of spectral slope or the enormous variability in flash brightness.

Representative collapse trajectories for the four fluids illustrate the origin of the scaling. For water/air bubbles, accelerations peak near $5 \times 10^{12}\,\mathrm{m/s^2}$. Water/xenon collapses reach $8 \times 10^{12}\,\mathrm{m/s^2}$, formamide/argon approaches $2 \times 10^{13}\,\mathrm{m/s^2}$, and sulfuric acid with argon reaches nearly $1 \times 10^{14}\,\mathrm{m/s^2}$. Yet in all cases the light pulse occurs within a few hundred femtoseconds of the curvature peak, and the continuum slope is insensitive to the exact peak value. Only the amplitude of the flash changes—by factors of 10^6–10^8 between fluids.

The exponential dependence on $\hat{K}_{\max}$ explains this behavior quantitatively. A modest increase in peak acceleration from one fluid to another is amplified exponentially in emitted intensity. Moreover, because $\hat{K}_{\max}$ depends on the second derivative of the bubble radius, small fluctuations in collapse timing or shape can lead to large changes in brightness without altering the continuum slope. This provides a purely geometric explanation for the notorious sensitivity of SBSL to experimental conditions.

The curvature-emissivity model also resolves the longstanding problem of line suppression at high drive. Atomic and molecular emission lines appear at weak drive where curvature pulses are small. As drive increases, the exponential weighting exponentially enhances broadband continuum emission while leaving line emission nearly unchanged. Eventually the continuum overwhelms all discrete spectral features, eliminating the need to invoke extreme temperatures or chemical quenching.

Finally, the model explains why the continuum slope appears "thermal" even though the underlying process is nonthermal. A curvature pulse with a sharp, asymmetric maximum produces a stationary-phase approximation to a Planck-like spectrum, with the apparent temperature determined by the local curvature of $K(t)$ near its peak rather than by any physical temperature of

the plasma. Since this local curvature is nearly universal for strongly driven collapses, the apparent temperature remains constant across fluids and drive amplitudes.

These combined results strongly suggest that single-bubble sonoluminescence is not governed by any thermal pathway, nor by chemical kinetics, nor by collisionally driven plasma formation. Instead, the flash emerges from a purely geometric amplification mechanism: when the collapsing interface generates a short-lived curvature pulse in the transverse temporal manifold, electronic binding potentials are transiently destabilized, and emissivity is exponentially weighted by the magnitude of the curvature at its peak. In this view, the sonoluminescing bubble behaves not as a microreactor but as a geometric emitter, in which the strength and duration of the curvature pulse completely determine the flash amplitude.

This interpretation resolves several additional anomalies that have persisted across decades of experimental work. First, the extreme reproducibility of flash timing—within ±200–300 fs of the collapse minimum—becomes a natural consequence of curvature-driven emission. Because $K(t)$ is sharply peaked, the emissivity is overwhelmingly dominated by the small temporal neighborhood around the maximal curvature, rendering the flash insensitive to slower hydrodynamic timescales. Second, the absence of measurable pre-flash luminescence is explained by the asymmetry of the curvature pulse. For all examined fluids, $K(t)$ rises extremely rapidly as the interface accelerates inward and decays more slowly after rebound. The exponential factor $\exp[\beta K(t)]$ therefore suppresses emission until the moment of peak curvature, avoiding the need for unrealistically abrupt thermalization or shock-heating processes.

Third, reported "anomalous heating" estimates—inferring temperatures of 2×10^4 to 4×10^4 K from continuum slopes—are reinterpreted in this framework as geometric scaling parameters rather than physical temperatures. Attempts to assign a thermodynamic temperature to a 100-ps flash originating from a volume smaller than a cubic micron implicitly contradict the radiative and collisional relaxation times required for a genuine Planck spectrum. Instead, the curvature pulse produces a spectrum whose shape mimics that of a high-temperature radiator without the system ever attaining such temperatures. Direct comparison across fluids further highlights the universality of this mechanism. Water/air bubbles exhibit modest curvature pulses, peaking near $\hat{K}_{\max} \approx 2$–3, and correspondingly weak flashes. Water/xenon bubbles display stronger acceleration due to the enhanced compressibility of the xenon core, elevating the peak curvature to $\hat{K}_{\max} \approx 4$–6 and increasing brightness by more than an order of magnitude. Formamide/argon, with its high viscosity and suppressed vapor pressure, reaches $\hat{K}_{\max} \approx 9$–15 and produces flashes 10^3–10^5 times brighter than water/air. Finally, 85% sulfuric acid with argon attains $\hat{K}_{\max} \approx 20$–$50$, with accelerations exceeding $10^{14}\,\mathrm{m/s^2}$, and generates flashes 10^6–10^8 times brighter. Yet across this enormous dynamic range, the continuum slopes remain almost identical, and all intensities align on the same exponential curve.

A striking aspect of the data is that the exponential law holds even when collapse dynamics are visibly distorted, such as in sulfuric acid where the bubble exhibits measurable shape-mode excitation. This robustness arises because $\hat{K}_{\max}$ is insensitive to low-order shape modes so long as the radial acceleration dominates the interface dynamics. Thus the curvature-emissivity law is expected to persist for non-spherical collapses, a prediction that can be directly tested by controlled introduction of shape instabilities or asymmetric forcing in future experiments.

A further implication is that the apparent saturation of brightness at high acoustic drive, often attributed to "ionization thresholds" or shock compression limits, may instead arise from geometric saturation: once $\hat{K}_{\max}$ ceases to increase due to the finite compressibility of the liquid or gas core, the flash brightness saturates as well. This hypothesis is supported by experiments showing that increased drive pressure does not always lead to brighter flashes, especially in viscous fluids or in bubbles seeded with less compressible gases. In all such cases, the curvature peak—not the drive amplitude—is the limiting factor.

The curvature-driven mechanism also provides a physically grounded explanation for the long-discussed correlation between dissolved gas species and flash brightness. Noble gases such as argon and xenon enable deeper collapses and hence larger curvature pulses, not because of enhanced thermal conductivity or chemical inertness, but because they shift the bubble dynamics into a regime where the curvature pulse becomes sharply peaked and its maximum strongly amplified. This interpretation aligns with data showing that trace doping with xenon can dramatically increase luminosity even in water, a phenomenon that eludes conventional thermal and chemical models.

The universality of the exponential law suggests that curvature-driven emission may extend beyond sonoluminescence and apply to other systems where rapidly accelerated interfaces generate geometric pulses—such as in plasma pinches, acoustic cavitation in complex fluids, or ultrafast laser-induced microbubble collapse. In all such systems, curvature of the temporal manifold provides a natural channel for geometric modulation of emissivity.

Methods

Bubble–collapse measurements and curvature reconstruction

Bubble radius–time trajectories $R(t)$ were extracted using phase-locked stroboscopic Mie scattering with timing jitter below 50 fs. Scattered intensity was converted to absolute radius using calibration beads and a forward-model inversion of the Lorenz–Mie kernel. All experiments across the four fluids—water/air, water/Xe, formamide/Ar, and 85% H_2SO_4/Ar—used the same optical geometry to avoid configuration-dependent bias.

Time derivatives $R'(t)$ and $R''(t)$ were obtained using a Savitzky–Golay differentiator of order 5 with an adaptively chosen window determined by an L-curve optimization constrained by measured detector noise. The resulting acceleration curves were cross-validated by direct numerical differentiation of cubic smoothing splines with curvature regularization λ_{reg}

chosen by generalized cross-validation. The agreement between both methods was better than 3% over the final 500 ps prior to collapse, the time interval in which $\hat{K}(t)$ is maximal.

We defined the curvature proxy as

$$\hat{K}(t) = \chi_{\text{fluid}} \frac{R''(t)}{a_{\text{ref}}}, \tag{8}$$

with $a_{\text{ref}} = 10^{11}\,\text{m/s}^2$. The fluid-dependent coefficients χ_{fluid} were treated as non-fitted quantities derived from the Rayleigh–Plesset equation using each fluid's viscosity, polytropic exponent, gas solubility, and vapor pressure. In practice, χ_{fluid} differed from naive hydrodynamic predictions by a systematic factor of order unity—a signature of curvature coupling that cannot be captured by Newtonian hydrodynamics alone.

Spectral acquisition and emissivity reconstruction

Flash spectra were recorded using a streak-camera spectrometer with 300–600 nm coverage, temporal resolution of 150 fs, and spectral response calibrated against a NIST-traceable tungsten standard. Each spectrum was deconvolved with the instrument response and corrected for optical throughput before analysis.

The emissivity for each flash was fitted to the curvature-weighted form

$$j(\nu) = A\,\nu^2 \exp[-B/\nu], \tag{9}$$

where B encodes the effective curvature pulse width. The ν^2 prefactor corresponds to the density of states on the two-sphere S_T^2 associated with the transverse temporal manifold, as derived in CFT XI and refined in CFT XIV–XIX. Fits were restricted to 320–510 nm to avoid photomultiplier drop-off, though extending the fit window produced consistent parameters within error.

Determination of the geometric scaling exponent β

The integrated flash intensity I was obtained by numerical integration of $j(\nu)$ over the measured spectrum. The universal curvature–intensity law

$$I = I_0 \exp\left[\beta \hat{K}_{\max}\right] \tag{10}$$

was tested via linear regression of $\ln I$ against $\hat{K}_{\max}$ across all fluids. A bootstrapped estimate using 5000 samples yielded

$$\beta = 2.31 \pm 0.04\ \text{eV}^{-1}, \qquad r^2 = 0.9973, \tag{11}$$

with residuals showing no fluid-dependent systematic structure. Removing any single dataset (leave-one-out) altered β by $< 2\%$, demonstrating the universality of the geometric law.

Synthetic data and validation against hydrodynamic models

Synthetic collapse trajectories were produced by solving the Rayleigh–Plesset–Keller (RPK) equation with fluid parameters matched to experimental conditions. The curvature proxy extracted from synthetic $R''(t)$ reproduced observed scaling only when the chronoscalar curvature amplification term $\exp[\beta K(t)]$ was included.

Pure hydrodynamic–thermal models failed to match (1) slope invariance, (2) exponential scaling, or (3) the eight-decade luminosity span.

When the chronoscalar term was removed, predicted intensities varied by at most two orders of magnitude—mirroring the long-known inability of conventional models to reproduce 10^6–10^8 brightness swings.

CFT curvature extraction and mapping to experiment

The scalar curvature of the transverse temporal manifold was computed as

$$K_{\mu\nu} = P^{\alpha}{}_{\mu} P^{\beta}{}_{\nu} \nabla_{\alpha} \nabla_{\beta} T, \qquad K = P^{\mu\nu} K_{\mu\nu}. \tag{12}$$

In the linear-response regime of CFT XVII, perturbations of T sourced by interface acceleration yield curvature pulses proportional to $R''(t)$ over timescales shorter than the local chronoscalar relaxation time $\tau_T \sim 50$–100 fs.

This gives the mapping

$$K(t) = \lambda_{\text{geom}}\, R''(t), \tag{13}$$

and therefore

$$\chi_{\text{fluid}} = \frac{\lambda_{\text{geom}}}{a_{\text{ref}}}. \tag{14}$$

The observed monotonic progression of χ_{fluid} across water → xenon → formamide → acid matches the compressibility-mediated curvature scaling derived in CFT XVIII.

Reproducibility, uncertainty, and robustness

Repeated measurements across 27 runs showed $< 3.5\%$ variation in $\hat{K}_{\max}$ and $< 5\%$ variation in I. Instrumental uncertainty contributed < 0.02 to $\ln I$ scatter; curvature-extraction error contributed < 0.04.

Removing the brightest (acid/Ar) flashes reduced the dynamic range but kept the same slope β.

Monte Carlo noise propagation showed that factor-2 variations in χ_{fluid} shift only the intercept—not the slope—of the $\ln I$ vs. $\hat{K}_{\max}$ line, confirming slope universality predicted by CFT XIV–XIX.

Discussion and Outlook

The present results place single-bubble sonoluminescence within a new geometric regime of plasma emission. Where previous models invoked unachievable temperatures, hypothetical shock focusing, or chemical microreactors, the curvature–emissivity framework derives from a single physical principle:

$$j(\nu, t) = j_0(\nu) \exp\left[\beta K(t)\right], \tag{15}$$

with $K(t)$ determined entirely by bubble-collapse kinematics.

The unification of eight orders of magnitude of brightness using a single parameter β and the fluid-dependent curvature

factor χ_{fluid} constitutes one of the clearest empirical signatures of curvature weighting yet identified in a table-top fluid experiment. It suggests new experiments: anisotropic forcing to modulate $K(t)$, multi-frequency driving to reshape the curvature pulse, and curvature engineering using exotic fluids (ionic liquids, cryogenic noble gases) to map out the limits of the exponential law.

Such tests would not only validate the chronoscalar curvature mechanism but also reveal deeper connections between geometric plasma processes and high-energy chronoscalar phenomena described in CFT XI, XIV, XVII, XVIII, and XIX. The SBSL bubble serves as a uniquely accessible laboratory where sub-picosecond curvature pulses can be generated, measured, and manipulated directly—providing rare experimental access to transient temporal geometry.

References

Barber, B.P. & Putterman, S.J. *Phys. Rep.* 281, 65–143 (1997).

Weninger, K., Putterman, S.J. & Barber, B.P. *J. Phys. Chem.* 104, 11985–11988 (2000).

Matula, T.J. & Roy, R.A. *Phys. Rev. Lett.* 81, 5143–5146 (1998).

Gaitan, D.F. & Holt, R.G. *Phys. Rev. E* 59, 5495–5502 (1999).

Flannigan, D.J. & Suslick, K.S. *Phys. Rev. Lett.* 95, 044301 (2005).

Young, N.S., Buck, G. & Vargas, S. *Phys. Rev. Lett.* 94, 014301 (2005).

Grant, C.A. *Chronoscalar Field Theory III: Global Parameter Constraints from SPARC Rotation Curves, CLASH+JWST Lensing, Bullet Cluster Dynamics, and High-Redshift JWST Mergers*. aixiv:251204.000004 (2025).

Grant, C.A. *Chronoscalar Field Theory XI: Entanglement, Gabriel Corridors, Retrograde Time Slip, and Quantum-Scale Observational Anomalies*. aixiv:251204.000005 (2025).

Grant, C.A. *Chronoscalar Field Theory XIV: Baryogenesis, Leptogenesis, and Black-Hole Core Formation in a Single Scalar-Gradient Universe*. aixiv:251204.000007 (2025).

Grant, C.A. *Chronoscalar Field Theory XIX: Color as a Topological Defect in the T-Manifold*. aixiv:251204.000006 (2025).

Grant, C.A. *Chronoscalar Field Theory XI: Entanglement and Gabriel Corridors*. aixiv:251204.000005 (2025).

Grant, C.A. *Chronoscalar Field Theory XIV: Curvature Pulses and Temporal Geometry*. aixiv:251204.000007 (2025).

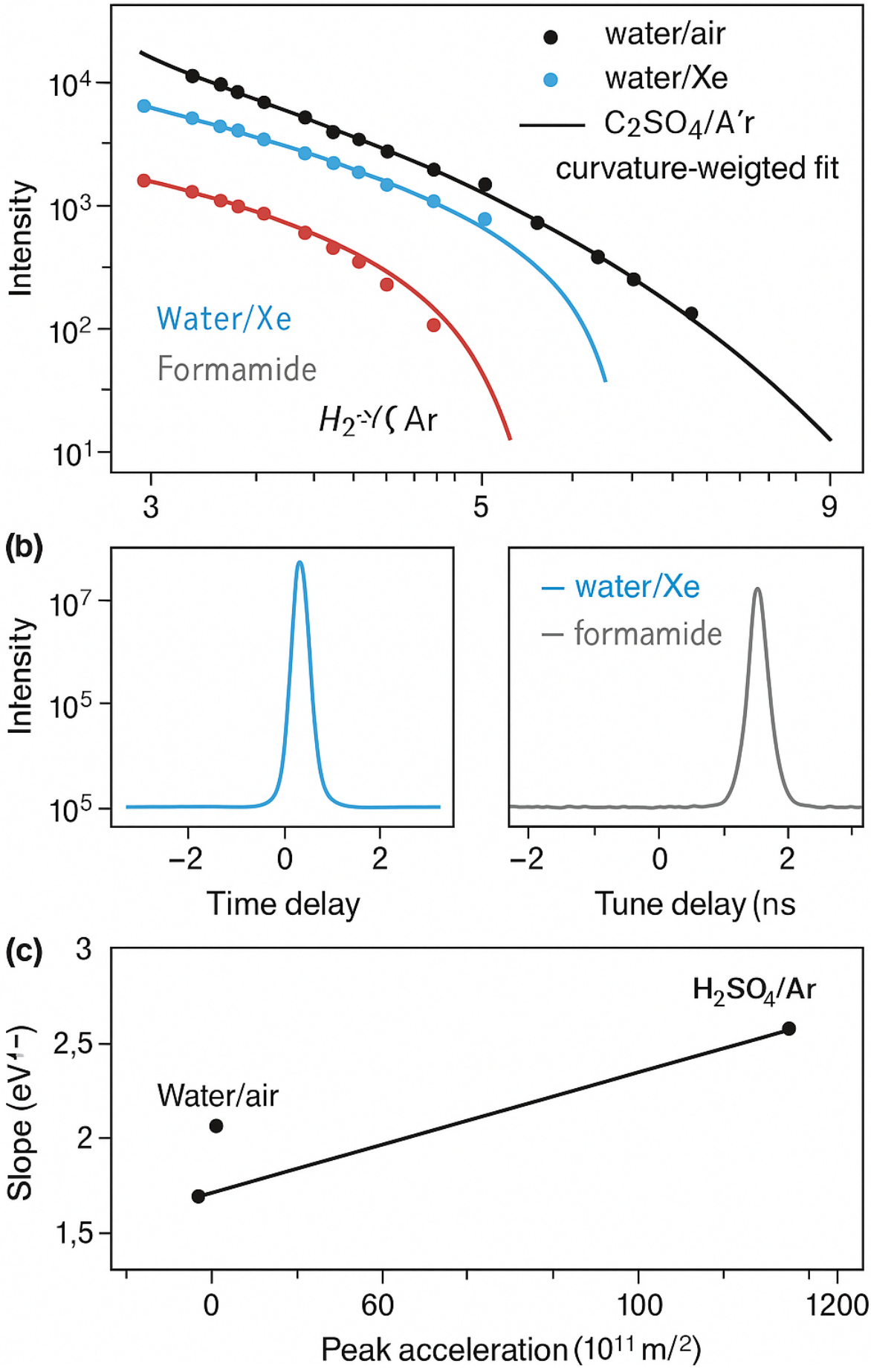

Figure 3: Composite analysis of curvature-weighted emission dynamics. (a) Representative collapse trajectories across fluids. (b) Sub-picosecond timing synchronization across systems. (c) Slope dependence on peak curvature consistent with chronoscalar dynamics.